

**Structure and function of the PiuA and PirA siderophore-drug
receptors from
Pseudomonas aeruginosa and *Acinetobacter baumannii***

Lucile Moynié¹, Alexandre Luscher^{2,3}, Dora Rolo^{3,4}, Daniel Pletzer⁵,
Antoni Tortajada¹, Helge Weingart⁵, Yvonne Braun⁵,
Malcolm G. P. Page⁶,
James H. Naismith¹ and Thilo Köhler^{2,3*}

¹University of St Andrews, United Kingdom

²Service of Infectious Diseases, University Hospital Geneva and

³Department of Microbiology and Molecular Medicine, University of Geneva, Switzerland

⁴ISGlobal, CRESIB, Hospital Clinic, Universitat de Barcelona, Spain

⁵Jacobs University, Bremen, Germany

⁶Basilea Pharmaceutica International Ltd, Basel, Switzerland

*To whom all correspondence should be addressed:

Department of Microbiology and Molecular Medicine

University of Geneva

1, Rue Michel Servet

CH-1211 Genève 4, Switzerland

Phone: +41 22 379 55 71

Fax: +41 22 379 57 02

E-mail: thilo.kohler@unige.ch

26 † Present address: Jacobs University, Bremen, Germany

27 Running title: Structure and function of siderophore-drug receptors

28 Keywords: *Pseudomonas aeruginosa*, *Acinetobacter baumannii*, siderophore-drug receptor

29

Abstract

The outer membrane of Gram-negative bacteria presents an efficient barrier to the permeation of antimicrobial molecules. One strategy pursued to circumvent this obstacle is to hijack transport systems for essential nutrients such as iron. BAL30072 and MC-1 are two monobactams conjugated to a dihydroxypyridone siderophore that are active against *Pseudomonas aeruginosa* and *Acinetobacter baumannii*. Here, we investigated the mechanism of action of these molecules in *A. baumannii*. We identified two novel TonB-dependent receptors, termed *Ab-PiuA* and *Ab-PirA* that are required for antimicrobial activity of both agents. Deletion of either *piuA* or *pirA* in *A. baumannii* resulted in 4 to 8 fold decreased susceptibility, while their overexpression in the heterologous host *P. aeruginosa* increased susceptibility to the two siderophore-drug conjugates by 4 to 32 fold. Crystal structures of PiuA and PirA from *A. baumannii* and their orthologues from *P. aeruginosa* were determined. The structures revealed a similar architecture, however structural differences between PirA and PiuA point to potential differences between their cognate siderophore ligands. Spontaneous mutants, selected upon exposure to BAL30072, harbored frame-shift mutations in either the ExbD3 or the TonB3 proteins of *A. baumannii*, forming the cytoplasmic membrane complex providing the energy for the siderophore translocation process. The results of this study provide insight for the rational design of novel siderophore-drug conjugates against problematic Gram-negative pathogens.

Word count: 221

Introduction

The outer membrane of Gram-negative bacteria is an efficient barrier that limits access of antibiotics to their targets. *Pseudomonas aeruginosa* and *Acinetobacter baumannii* are characterized by especially low outer membrane permeability due to slow influx across porin-channels and relatively rapid efflux via numerous efflux systems of the Resistance-Nodulation-Division (RND)-type (1). There have been several attempts to exploit alternative transport mechanisms to overcome this permeability barrier (2). In this view the TonB-dependent receptors (TBDRs), able to transport siderophores or vitamin B12 in Gram-negative organisms (3), as well as carbohydrates, cations and thiamine (4), are particularly attractive. Due to their high affinity binding sites, substrates are transported even at low substrate concentrations. Furthermore they can perform concentrative uptake (uphill transport) for enterochelin (5) and vitamin B12 (6), and accommodate large substrate molecules including cobalamines, heme, or peptidic siderophores such as pyoverdine. In contrast to porin-mediated passive diffusion, the uptake via the outer membrane TBDRs requires energy, derived from the proton motive force, and transmitted via the TonB-ExbB-ExbD complex located in the cytoplasmic membrane.

In order to hijack these uptake systems, conjugates between antibiotics and siderophore molecules have been designed. So far, most success has been obtained with beta-lactams, since their target is located in the periplasmic space to which most of the siderophores are delivered (3). The iron-binding moiety of beta-lactam siderophore conjugates is frequently a small catechol-type siderophore such as dihydroxypyridone or a mixed catechol/hydroxamate (7). Such conjugates have been developed with aminopenicillins (8), cepheems (KP-736, S-649266) (9-11) and monocyclic beta-lactams (pirazmonam, BAL30072, MC-1) (12-15). In particular the monobactam conjugates show potent activity against the Gram-negative non-fermenters *P. aeruginosa* and *A. baumannii* (15-18).

A. baumannii is a nosocomial pathogen associated with severe infections in immunocompromised hosts (19). Besides its chromosomally encoded AmpC-type beta

lactamase (20), *A. baumannii* frequently harbors class B and D carbapenemases (21) and extended-spectrum beta-lactamases (ESBL) of the PER, GES and VEB types (22). RND-type efflux systems including AdeABC (23), AdeIJK (24) and AdeFGH (25) further contribute to the multi-drug resistance phenotype of clinical isolates. *A. baumannii* harbors between 21 and 27 TonB-dependent receptors, compared to 35 in *P. aeruginosa* (26). So far, only FhuE (27) and BauA (28), the receptor for the siderophore acinetobactin (29, 30), have been characterized in *A. baumannii*.

In this study we identified two novel TonB-dependent receptors of *A. baumannii*, termed PiuA and PirA, required for the activity of two monocyclic beta-lactam siderophore conjugates. When expressed in *P. aeruginosa* both receptors confer hypersusceptibility to the two drugs. The first crystal structures of PiuA and PirA were obtained together with their orthologues from *P. aeruginosa*. Although showing a similar overall structure, there were marked differences in their putative substrate binding sites. The data should provide insight for the future rational design of novel siderophore-drug conjugates.

Materials and Methods

Bacterial strains and growth conditions. Strains and plasmids used in this study are listed in Table 1 and primers used are shown in Table S1. *A. baumannii* strains were grown in double strength Yeast Tryptone (dYT) broth and *E. coli* and *P. aeruginosa* in Lysogeny Broth (LB) at 37 °C with shaking (220 rpm). *E. coli* XL-1 Blue and DH10B were used as cloning hosts. *E. coli* ST18 was the donor strain for biparental matings, requiring supplementation with 50 µg/ml 5-aminolevulinic acid. Gentamicin (25 µg/ml) or kanamycin (25 µg/ml) were added for plasmid carrying strains. Minimum inhibitory concentration (MIC) determinations were performed in Mueller-Hinton (MH) broth according to CLSI guidelines (31), and were repeated at least on three different occasions.

Mutant selection and growth assay. Spontaneous mutants of the fully sequenced *A. baumannii* strain 307-0294 were selected on LB-agar plates supplemented with BAL30072.

Individual colonies were picked and grown in the absence of antibiotic. MICs were determined and strains with decreased susceptibility to BAL30072 were retained for further analysis. The growth of mutant strains was performed in microtiter plates in a total volume of 200 μ l. Strains were grown for 7 h in LB-broth with shaking (250 rpm) at 37 °C. Cultures were diluted to an OD₆₀₀ of 0.015 and 4 μ l inoculated into 196 μ l of MH-broth. Growth was followed in a BioTek Synergy 1 plate reader at 37 °C with shaking 1 min before hourly measurement of the optical density at 600 nm. Growth curves represent the average OD₆₀₀ values for duplicate cultures.

PCR amplifications and DNA modifications. PCR primers are listed in Supporting Information (Table S1). All primer sequences were based on the genome of *A. baumannii* ATCC 19606 (GenBank: NZ_ACQB000000000). Screening PCR reactions were carried out using the DreamTaq DNA polymerase (Thermo Scientific) in accordance with the manufacturer's instructions and optimized annealing temperature for each primer set. For screening PCR reactions, bacterial cells were boiled at 95°C for 5 min and subsequently pelleted at 13,000 rpm for 1 min. Phusion DNA polymerase (Thermo Scientific) was used for high fidelity PCR reactions (supplemented with 5% DMSO). Restriction digestions were performed using Thermo Scientific restriction enzymes according to the manufacturer's instructions at the appropriate temperature. All ligation reactions were carried out at room temperature using Thermo Scientific T4 DNA ligase. DNA purifications were either performed using the GeneJET PCR purification or the GeneJET Gel extraction kit (Thermo Scientific) following the manufacturer's instructions.

Construction of *pirA* and *piuA* knockout mutants in *A. baumannii*. The generation of unmarked knockout mutants was based on the protocol described by Hoang *et al.* (32). Briefly, DNA fragments of 500-700 bps were PCR-amplified using primer pairs A1/A2 and B1/B2, respectively (Table S1). For deletion of *pirA*, the up- and downstream regions flanking the gene were PCR-amplified. For knockout of *piuA*, the amplified fragments were located in the 5' and 3' regions of the genes. After amplification, the obtained A- and B-fragments were gel-purified and approximately 40 ng of each fragment was used in a PCR fusion with primers A1 and B2,

which share an 18-bp homologous region. The resulting fusion products were gel-purified and further cloned into the suicide vectors pEX18Gm via *HindIII*/*EcoRI* restriction sites (*pirA*) and pEX18Km via *Sall*/*EcoRI* (*piuA*). The cloned knockout fragments were verified by sequencing. The replacement vectors were mobilized into *A. baumannii* via biparental conjugation and the generation of the unmarked mutants was carried out as previously described (33). In order to confirm a gene deletion, locus-specific primers (out1, out2) were designed, which bind up- and downstream of the gene, and used for amplification of the knockout region. Sequencing of the obtained PCR fragments confirmed successful deletion of the genes.

Construction of expression plasmids. The *piuA* and *pirA* coding regions were amplified by PCR from genomic DNA of *P. aeruginosa* reference strain PAO1. The *piuA* coding region was amplified with primers *piuA*-Xba and *piuA*-Hind and cloned as a 2,540 bp *XbaI*-*HindIII* DNA fragment into the expression vector pIApX2 yielding plasmid ppiuA1.1. Deletions of residues 73-76 from loop NL1 (ppiuA Δ L1.1) were constructed with a modified protocol of the QuickChange method (34) using primers *piuA*- Δ 1 and *piuA*- Δ 2. The *pirA* coding region was amplified as a 2,498 bp DNA fragment obtained with primers *pirA*-Bam and *pirA*-Hind2 (Table S1). The PCR product was digested by *Bam*HI and *Hind*III and cloned into pIApX2 yielding plasmid ppirA1.1. The coding regions of *piuA* (A1S_0474) and *pirA* (A1S_0980) were amplified by PCR from genomic DNA of *A. baumannii* strain 307-0294 (provided by Prof. T.A. Russo, SUNY, Buffalo, USA), using primers listed in Table S1. The 2,436 bp-long *piuA* fragment was digested with *Eco*RI and *Pst*I and ligated to *Eco*RI and *Pst*I cleaved vector pEX1.8 yielding plasmid ppiuA-Ab6.3. The 2,557 bp-long *pirA* fragment was cleaved with *Xba*I and *Pst*I and ligated to plasmid pIApX2 cleaved with the same restriction enzymes, yielding plasmid ppirA-Ab4.1. Plasmids were transferred into *P. aeruginosa* by electroporation. The *piuA*-Ab gene was further subcloned by *Bam*HI-*Pst*I digestion into the *A. baumannii* expression vector pBAV1K-5T-gfp (35) (kindly provided by Prof. G. Wilharm, Robert Koch Institut, Werningerode, Germany) yielding plasmid ppiuA-Ab7.1. The *piuA*-Ab gene was further subcloned by *Xba*I-*Pst*I digestion into pBAV1K-5T-gfp, yielding plasmid

ppirA-Ab3.1. PCR conditions were as follows: denaturation at 95°C for 2 min, followed by 27 cycles of 95°C for 20 s, 57°C for 30 s, 72°C for 2 min and a final extension at 72°C for 4 min. Plasmids were introduced into *P. aeruginosa* and *A. baumannii* by electroporation. Plasmid containing colonies were selected on LB-agar supplemented with carbenicillin at 200 mg/L (*P. aeruginosa*) or kanamycin at 50 mg/L (*A. baumannii*).

Cloning, overexpression and purification of PiuA and PirA from *P. aeruginosa* and *A. baumannii*. Position of the signal peptide cleavage site of the proteins was predicted with Signal P4.0 (36). The coding sequence of the mature protein *Pa*-PiuA (PA4514) was amplified from PAO1 genomic DNA using primer pairs *Pa*-PiuA-F/R (Table S1) and Pfu DNA polymerase. The PCR product was digested by *Bsp*HI and *Eag*I restriction enzymes and cloned into vector pET20b using restriction enzymes *Nco*I and *Eag*I so that the protein was expressed with a PelB signal sequence for the outer-membrane localisation and a non-cleavable C-ter His₆ tag. Codon-optimized *Pa*-PirA (PA0931) with a C-terminal non-cleavable His₆ tag was purchased from DNA2.0 and inserted into vector pET20b using *Hind*III and *Eco*RV restriction sites.

The coding sequences of the mature proteins *Ab*-PiuA and *Ab*-PirA were amplified by PCR from *A. baumannii* strain ATCC 19606 using KOD DNA polymerase (Novagen) and the primer pairs *Ab*-PiuA-F/R and *Ab*-PirA-F/R (Table S1). Both genes were cloned with an N-terminal tobacco etch virus (TEV) protease cleavable His₇-tag in vector pTAMAHISTEV using *Nco*I and *Bam*HI restriction sites. The pTAMAHISTEV expression vector was obtained by replacing the PelB signal peptide of plasmid pPELBHISTEV (courtesy of Dr. Huanting Liu, University St. Andrews) by the TamA signal peptide as described by Liu *et al.* (37).

Proteins were over-expressed in *E.coli* strains C43 (DE3) or BL21 (DE3). Cells were grown at 37 °C in LB medium containing 100 mg/L ampicillin until an OD₆₀₀ of 0.7 and then induced with 0.4 mM IPTG at 25°C overnight.

For *Pa*-PiuA and *Pa*-PirA, harvested cells were re-suspended in lysis buffer (50 mM sodium phosphate pH 7.5, 250 mM NaCl, 10% glycerol, 100 µg/ml lysozyme and 20 µg/ml DNase).

Cells were lysed by two passages through a cell disruptor at 30 Kpsi (Constant systems). Unbroken cells were removed by centrifugation (20 min at 10,000xg) and membrane fractions isolated by ultracentrifugation (100,000xg, 1 h). The supernatant was discarded and inner membrane proteins were solubilised in buffer 1 (50 mM sodium phosphate pH 7.5, 250 mM NaCl, 10% glycerol and 1% (w/v) N-lauroylsarkosine (Sigma). The insoluble outer membrane fraction was isolated by ultracentrifugation (100,000xg, 1h) and outer membrane proteins were solubilised in buffer 2 (50 mM sodium phosphate pH 8, 250 mM NaCl and 7% (v/v) octylpolyoxyethylene (octylPOE), Bachem). Insoluble material was removed by ultracentrifugation (100,000xg, 1h). The supernatant was applied to a charged Histrap Nickel Sepharose, high performance column (GE Healthcare) equilibrated with 1% octylPOE (v/v), 250 mM NaCl, 10 mM Imidazole and 50 mM sodium phosphate pH 8, washed with the same buffer containing 15 mM imidazole. Protein was eluted with a linear gradient of imidazole (5 to 150 mM). Fractions containing the protein were pooled, dialysed against 50 mM Tris pH 8.4 and 1% octylPOE and loaded on a Q-source column equilibrated with the dialysis buffer and eluted with a linear gradient of 0-600 mM NaCl over 12 column volumes. Fractions were pooled and loaded on a Superdex S200 gel filtration column (GE Healthcare) equilibrated with 10 mM Tris pH 8, 150 mM NaCl, and 0.45% (v/v) n-octyltetraoxyethylene (C8E4) (Bachem). Protein fractions were pooled and concentrated to 8 mg/ml.

Expressions and initial purification steps of *Ab*-PiuA and *Ab*-PirA were the same as for *Pa*-PiuA and *Pa*-PirA. After a first IMAC column, imidazole was removed by dialysis (50 mM Tris pH 8, 250 mM NaCl, 10% glycerol, 2 mM mercaptoethanol and 1% octylPOE) before adding the TEV protease to cleave the His₇ -tag. Protein was applied to a second IMAC column followed by a Superdex S200 gel filtration chromatography (GE Healthcare) (10 mM Tris pH 8, 150 mM NaCl, 0.45% C8E4). Protein fractions were pooled and concentrated to 10 mg/ml.

Crystallization and Structure Determination. Crystals of *Pa*-PiuA appeared at 20°C after several days by mixing 1 µl of protein solution (8 mg/ml) with 1 µl of reservoir solution containing 32% polyethylene glycol (PEG) 400, 0.05 M Tris pH 8.5, 0.05 M sodium sulphate

216 and 0.05 M lithium chloride. *Pa*-PirA crystals were obtained at 20°C by mixing 1.5 µl of the
 217 protein solution (7.5 mg/ml) containing 2.5 mM n-dodecylphosphocholine (Anatrace) with 1
 218 µl of reservoir solution containing 17% PEG 3350, 0.2 M magnesium chloride, 0.1 M Tris pH
 219 7. Crystals were frozen with the same solution containing 25% PEG 400.

220 Crystals of *Ab*-PiuA appeared at 20°C after several days by mixing 1 µl of protein solution (10
 221 mg/ml) with 1 µl of reservoir solution containing 1 M diammonium hydrogen phosphate, 0.1 M
 222 sodium acetate pH 4.6. Crystals were cryo-protected by supplementing the mother liquor with
 223 30% sucrose. Prior to crystallisation, Fe³⁺-enterobactin was added to *Ab*-PirA at a final
 224 concentration of 1 mM before loading on a Superdex S200. *Ab*-PirA crystals appeared a week
 225 after mixing at 20°C 1 µl of protein solution (7 mg/ml) with 1 µl of reservoir solution containing
 226 16% PEG 8000, 0.15 M magnesium sulfate and 0.1 M bicine pH 9.

227 Data were collected at the beamlines IO4, IO3 at the Diamond light source Oxfordshire and
 228 ID14-4 at ESRF. Data were processed with XIA2 (38-42). Structure of *Pa*-PiuA was solved by
 229 molecular replacement using the coordinate of FhuA (2FCP) (43) as a model with the program
 230 PHASER (44). Structure of *Ab*-PiuA was solved using *Pa*-PiuA coordinates and structures of
 231 *Pa*-PirA and *Ab*-PirA were solved using FepA coordinates (1FEP) (45). Models were adjusted
 232 with COOT (46) and refinement was carried out using REFMAC in the CCP4 program suite
 233 with TLS parameters (47). Final refinement statistics are given in Table S2. Atomic coordinates
 234 and structure factors have been deposited in the Protein Data Bank (5fok, 5fp2, 5fp1, 5fr8).
 235 The quality of all structures was checked with MOLPROBITY (48). Figures were drawn using
 236 PyMOL (Version 1.8 Schrödinger, LLC).

237 **Whole genome sequencing.** Samples were sequenced on an Illumina MiSeq V2 instrument
 238 as 2 x150 paired-end reads. Assembly and analysis was performed off-instrument using
 239 CLCBio Genomics Workbench v 6.5 (Cambridge, MA). Detection of SNPs / indels was
 240 accomplished through mapping to a parent reference assembly using the same parameters.
 241 Quality based SNPs were detected at a minimum frequency of 80% using default criteria and
 242 verified by examination of *de novo* assembly. Annotation of parental strain was accomplished

through ORF calling using Prodigal software and BLAST analysis at NCBI for regions of interest. Sequence analyses were performed using the BLAST algorithm on genomic data provided by the MIST2.2 database (mistdb.com).

Results

Identification of PiuA and PirA orthologues in *A. baumannii*. We (49) and others (15) previously identified the TonB-dependent receptors (TBDR) PiuA and PirA, as important to the activity of the siderophore-drug conjugates BAL30072 and MC-1 in *P. aeruginosa*. Since BAL30072 also shows potent activity towards *A. baumannii* (14, 18, 50), we attempted to identify its mechanism of action in this organism. We performed a homology search for potential orthologues of PiuA and PirA on the genome of *A. baumannii* reference strain ATCC19606. The BLAST algorithm identified two uncharacterized ORFs, A1S_0474 and A1S_0980 (ATCC 17978 numbering) as the closest hits, sharing amino acid identities of 44% with PiuA and 51% with PirA of *P. aeruginosa*, respectively. Both genes have been shown to be preceded by putative Fur binding sites (A1S_0474: GCGAATAATAATAATTCTTATTTAT and A1S_0980: GATATTGTTAATAATTATCATTATT) (51), suggesting regulation by iron-availability via the Fur iron uptake regulator. Downstream of the *piuA* gene of *A. baumannii*, we identified an ORF (A1S_0473) showing 52% amino acid identity with *piuC* from *P. aeruginosa* and *ybiX* from *E. coli* (Fig. 1). The corresponding proteins belong to the family of Fe(II)-dependent oxidoreductases (52) and their co-localization with *piuA* might indicate that they act on the natural substrate transported by PiuA/FiuA. In contrast, the genetic environment of the *pirA* region of *A. baumannii* is different from those in *P. aeruginosa* and *E. coli* (Fig. 1). The *pirA* gene in *A. baumannii* is preceded by *nfuA*, coding for an Fe-S containing protein involved in intracellular iron utilization and oxidative stress response (53). In *P. aeruginosa* the gene for the secondary enterobactin transporter PirA is located next to a two-component system comprising the transcriptional regulator PirR (PA0929) and the sensor kinase PirS

(PA0930) (54). The closest orthologue of PirA in *E. coli* is the ferric-enterobactin transporter FepA, whose gene is embedded within the enterobactin biosynthesis region (not shown in Fig. 1). Based on these evidences, we adopted the nomenclature from *P. aeruginosa* and termed these proteins PiuA (A1S_0474) and PirA (A1S_0980), designated below as Ab-PiuA and Ab-PirA.

PiuA and PirA contribute similarly to siderophore-beta-lactam activity in *A. baumannii*.

To test the involvement of PiuA and PirA in the activity of BAL30072 and MC-1 against *A. baumannii*, we constructed deletion mutants in the *piuA* (A1S_0474) and *pirA* (A1S_0980) genes in *A. baumannii* strain ATCC19606. Both the *piuA* and the *pirA* mutants showed 2-8 fold increases in MICs for both drug-conjugates, in agreement with decreased transport in the individual mutants. The *piuA* - *pirA* double mutant showed a further increase in MICs, which was more pronounced for MC-1 than for BAL30072 (Table 2). This suggests that in the wild type strain and under the conditions of the MIC assay, both receptors have a basal expression level and may contribute similarly to the uptake of BAL30072 and MC-1. This is in contrast to the situation in *P. aeruginosa*, since deletion of *pirA* in PAO1 has no effect on the susceptibility to BAL30072 and MC-1 and the contribution of this TBDR is seen only in a *piuA* deletion background (15).

PiuA and PirA from *A. baumannii* are functional in *P. aeruginosa*.

To test whether the *A. baumannii* proteins are functional in *P. aeruginosa*, plasmids ppirA-Ab4.1 and ppiuA-Ab6.3 expressing respectively the *pirA* and *piuA* genes of *A. baumannii* from a constitutive or an inducible promoter, were transferred into *P. aeruginosa* strain PAO1 and into a *piuA* deletion mutant. While expression of the vector plasmids alone had no significant effect on BAL30072 or MC-1 MICs, the expression of both *piuA* and *pirA* from *A. baumannii* conferred increased susceptibility to these conjugates in *P. aeruginosa*. As expected, susceptibility to aztreonam (ATM) was not affected by overexpression of the TBDR genes (Table 3). Similar results were obtained in a *piuA* deletion strain showing a 32 to 64-fold increase in susceptibility to BAL30072 and MC-1, when the *pirA* gene of either *P. aeruginosa* or *A. baumannii* were overexpressed.

However, *Ab*-PiuA expression from plasmid ppiuA-*Ab*6.3 did not seem to confer increased susceptibility on the *piuA* deletion strain (Table 3). A possible explanation is that the induced expression level of *Ab*-PiuA in the *piuA* deletion strain might be insufficient to restore wild type susceptibility.

Structure comparison of PiuA and PirA from *P. aeruginosa* and *A. baumannii*. The sequence alignment of the PiuA and PirA orthologues revealed high conservation within the putative substrate binding domains NL1 (PiuA and PirA), NL2 and NL3 (PirA) (Fig. 2). The structures of PiuA and PirA from *P. aeruginosa* and *A. baumannii* have been solved. As expected, these structures were similar to other TBDRs, sharing a two domain organization, consisting of a 22-stranded transmembrane β -barrel (green ribbon) and an N-terminal plug domain (blue ribbon) folded inside the barrel (Fig. 3).

As often observed with TBDRs, several extracellular loops were missing in the *Pa*-PiuA structure. Loops NL1 (83-90), L7 (505-526) and L8 (560-567) could not be modelled due to high flexibility of these regions. In contrast, the equivalent extracellular loops were present in the structure of *Ab*-PiuA, maybe due to the presence of a phosphate ion which coordinated with Glu73 of NL1, Asp303 of L4, Arg316 of β 8 and His697 of L11. Structural comparison of *Pa*-PiuA and *Ab*-PiuA (root-mean-square-deviations (r.m.s.d) of 1.3 Å for 616 aligned C α atoms)) showed differences in the length and position of several extracellular loops (Fig. 4 and Fig. S1). *Ab*-PiuA contained additional amino acids in loops L7 and L9, but less in L6 and L8 when compared to *Pa*-PiuA. Strikingly, loop L7 of *Ab*-PiuA folded inside the barrel close to the top of the plug domain (Fig. 4 and Fig. S1). A mutant protein with five amino acids (EGGNP; position 73-76) deleted from loop NL1 was generated in PiuA from *P. aeruginosa*. When expressed in strain PAO1, the NL1 deletion mutant was unable to confer hypersusceptibility to BAL30072, as observed with the PiuA wild type protein (Table 3). We conclude that loop NL-1 is likely involved in the initial binding of BAL30072 in PiuA.

Comparison with other TBDRs showed that the closest structural relatives of PiuA are the pyochelin (FptA) and pyoverdine (FpvA) receptors of *P. aeruginosa* (55, 56) with a r.m.s.d. of

1.84 Å (567 aligned C_α atoms) and 1.99 Å (555 aligned C_α atoms), respectively and the *E. coli* ferrichrome-iron receptor FhuA with an r.m.s.d. of 1.83 Å (600 aligned C_α atoms) (43, 57) (Fig. S1).

As for PiuA, the extracellular loops of PirA from *P. aeruginosa* were highly flexible, and the structural analysis of *Pa*-PirA was focused on the structure of PirA from *A. baumannii*, where these loops were experimentally located. PirA was similar to the ferric-enterobactin receptor FepA of *E. coli* (45) with an r.m.s.d. of 1.09 Å (618 aligned C_α atoms), as expected from the elevated sequence similarity (51% amino acid identity) (Fig. S1). This is consistent with a previous report identifying PirA of *P. aeruginosa* as a secondary transporter of ferric-enterobactin (54).

Selection of *A. baumannii* mutants with decreased susceptibility to BAL30072. We investigated the possibility of resistance emergence in *A. baumannii*. Colonies of strain 307-0294 and ATCC19606 able to grow in the presence of BAL30072 concentrations of 4 or 8 µg/ml were obtained at frequencies of 7×10^{-8} to 7×10^{-9} . After determining their susceptibility profile, we selected colonies which presented increased MICs of BAL30072 and MC-1 but unchanged MICs of aztreonam (ATM). Mutations in such colonies are expected to affect mechanisms specific to the siderophore-drug conjugate. Three out of six clones (R4, R5, R6) obtained with strain 307-0294 and none of the 8 clones tested from strain ATCC19606 fulfilled this criterion (Table 4). Therefore clones R4, R5 and R6 were selected for further analysis and submitted to whole genome sequencing. Mapping of the reads on the genome of strain 307-0294 revealed a single, but distinct mutation in each of the three strains. Mutant R4 had acquired a frame shift mutation (insertion of A at position 9) in the *exbD3* gene, while mutations in clones R5 (deletion of A at position 319) and R6 (insertion of A at position 243) resulted in frameshift mutations in the *tonB3* gene (Table 4). Interestingly, the *tonB3* but not the *tonB1* and *tonB2* genes (Fig. S2), have recently been shown to be induced under iron-limiting conditions (58). The TonB3-ExbB3-ExbD3 system could therefore be a likely candidate for providing energy to PiuA and PirA siderophore receptors in *A. baumannii*.

Decreased growth rate of spontaneous *exbD3* and *tonB3* mutants of *A. baumannii*. We observed that the spontaneous mutants R4, R5 and R6 formed slightly smaller colonies than the wild type when grown on LB-agar plates. To assess whether the mutations in the energy transducing TonB3 system impose a fitness cost, we compared the growth of the mutants to the wild type strain in MH-broth. As shown in Fig. 5, *tonB3* (R5 and R6) and the *exbD3* (R4) mutants were characterized by a longer lag-phase and a lower final cell density after 20 h growth when compared to the wild type. When the growth medium was supplemented with Fe(II)Cl₂ at a final concentration of 20 μM, the growth phenotype of mutants R4-R6 could be restored to reach nearly wild type levels. The data suggest that TonB3-ExbB3-ExbD3 is important for siderophore-mediated Fe³⁺ acquisition and that the fitness of such mutants is likely to be severely decreased *in vivo*, where iron availability is limited.

Discussion

In this study, we have identified two siderophore receptors, termed *Ab-PiuA* and *Ab-PirA* that are very likely involved in transport of the siderophore-monosulfactam conjugates BAL30072 and MC-1 into *A. baumannii*. The number of TBDRs found in different strains of *A. baumannii* ranges from 21 to 27 (compared to 35 in *P. aeruginosa*) (26). The close phylogenetic relation between *Acinetobacter* and *Pseudomonas* prompted us to search in *A. baumannii* for orthologues of the previously identified TonB-dependent receptors PiuA and PirA from *P. aeruginosa* (15, 59). For each of these proteins, we identified one orthologue (>40 % amino acid identity). The highest similarity was found within the putative substrate-binding sites located in the N-terminal region of the TBDRs (Fig. 2).

A transcriptome analysis performed in *A. baumannii* strain ATCC17978 recently showed that expression of both *piuA* and *pirA* are induced under iron-limiting conditions (51). *A. baumannii* strains harbor at least three distinct siderophore clusters, one of them being the acinetobactin biosynthesis operon. However, neither PiuA nor PirA are part of these clusters. This suggests that the two TBDRs are likely involved in the uptake of xenosiderophores, although the substrate(s) of PiuA has not been identified. The closest orthologue of PiuA in *E.*

coli is Fiu (35% amino acid identity), a TBDR also involved in the uptake of cephalosporins conjugated to catechol-siderophores (12, 13).

PirA is an orthologue of the enterobactin receptor FepA in *E. coli* (51% amino acid identity). Enterobactin is a tri-catechol siderophore produced by several enterobacterial species. However, the FepA receptor does not seem to play a role in the transport of catechol-based siderophore-drug conjugates in *E. coli* (12, 13), but it can transport beta-lactams linked to enterobactin (60, 61).

It is assumed in the design philosophy that BAL30072 interacts with the siderophore-receptors PiuA and PirA in a similar manner to their natural siderophores. However, the structures of the loops differ between the orthologous proteins from the two organisms. There are even larger differences between the loop structures of PirA and PiuA (Fig. S1). Since the natural siderophores of PiuA and PirA have not been known, we rely on comparisons with known complexes to inform us on the recognition elements. The binding site of known siderophore-receptors is in general formed by loops NL1, NL2, NL3 of the plug-domain, loops L3, L7, L11 and strands β 7, β 8, β 9 of the β -barrel (Fig. 2) (43, 55, 62).

The closest structural homologues of PiuA are FptA, FpvA and FhuA and their complexes with cognate siderophores show a cluster of aromatic and positively charged residues (Fig. 4). The side-chains of Tyr239 on loop L3 of *Pa*-PiuA and Trp298 in β 7 of *Ab*-PiuA have a similar position as Trp362 in FpvA and Met271 in FptA; both involved in siderophore binding. Tyrosines 307 and 296 on the loop β 7 of *Pa*-PiuA and *Ab*-PiuA occupy an equivalent position to FpvA Trp391 and FhuA Tyr116. A positively charged residue on β 8 (Lys329 for *Pa*-PiuA and Arg316 for *Ab*-PiuA) is in the same position as the side-chain of Lys344 in FhuA. Trp498 present in the loop L7 of *Ab*-PiuA occupies the same volume as Tyr231 and Phe115 in NL3 of FpvA and FhuA, respectively. A tyrosine/histidine couple (residues 694/697 in *Ab*-PiuA and 697/700 in *Pa*-PiuA) superimposes with Phe795 and Tyr796 in FpvA and Phe704 and Tyr707 in FhuA. We note that a phosphate ion is found in the *Ab*-PiuA structure where it is coordinated by Arg316 and His697. There are important differences however between *Pa*-PiuA and *Ab*-PiuA. In particular loops NL2 and NL3 are shorter in *Pa*-PiuA while NL1 extends above the

plug domain of *Ab*-PiuA (Fig. 3). Consequently NL1 in *Ab*-PiuA would clash with the siderophore location seen in FpvA, FptA and FhuA (Fig. S1). This may reflect a genuine difference with functional consequence or simply an inactive conformation.

Although there is no structure for the siderophore complex of FepA from *E. coli*, several binding and mutation studies have been reported (63) (64, 65). These studies suggest a biphasic binding kinetic with an initial binding site in the loop extremities and a secondary site deeper inside the barrel leading to the translocation. Loops L2, L4, L7, L8, L10 and L11 were found to be involved in the binding of ferric-enterobactin (45) (66). These loops are different in structure and sequence to those found in PirA, consistent with the observation that FepA does not transport BAL30072. Interestingly, it also indicates that PirA which can recognise enterobactin may use a different constellation of residues than FepA. The presumed second binding site, on top of the plug domain, is highly conserved between the two PirAs and FepA. Deletion of loops NL1 or NL3 in FepA or mutation of the conserved Trp101 in NL3 (corresponding to Trp 111 and 110 in *Ab*-PirA and *Pa*-PirA) drastically decreased the uptake of ferric-enterobactin (65, 66). Other key residues known to be important in FepA are Tyr260 of L3 (262 in *Ab*-PirA and 264 in *Pa*-PirA), Arg316 on β 7 (*Ab*-PirA R320 and *Pa*-PirA R321) and Tyr478 of L7 (*Ab*-PirA Tyr478 and *Pa*-PirA 479), which are conserved in PirA. As in FepA, loops L3, L4, L7 and L10 cover the top of the barrel making the plug domain less accessible than for the other TBDRs.

TBDRs interact with the cytoplasmic membrane protein TonB, which transmits energy derived from the proton gradient to the receptor via interaction with the N-terminal TonB-box, to drive substrate transport (Fig. S2). *A. baumannii* harbors three distinct chromosomally encoded TonB systems of which TonB3-ExbB3-ExbD3 was recently shown to be iron-regulated (58). Spontaneous resistant clones able to grow on >4 mg/L of BAL30072 carried frame-shift mutations in *tonB3* or *exbD3* (Fig. S2). It is therefore highly likely that the TonB3-ExbB3-ExbD3 system is interacting with PiuA and PirA to provide the energy for the uptake of BAL30072 and MC-1. Of note, the MICs of BAL30072 for the *tonB3* and *exbD3* mutants were higher than those for the individual TBDR mutants *piuA* and *pirA* or the *pirA-piuA* double mutant

(compare values in Table 2 and 4). Although the strain background is different (ATCC19606 vs 307-0294), it suggests that additional TBDRs could be involved in transport of siderophore drug conjugates in *A. baumannii* strain 307-0294. This assumption would also explain the selection of *exbD3* and *tonB3* mutants at 4 mg/L of BAL30072, which display higher MICs than the individual *pirA* and *piuA* mutants in strain ATCC19606.

The *A. baumannii tonB3* and *exbD3* mutants selected in strain 307-0294 on BAL30072 showed decreased growth rates under iron-limiting conditions. A similar growth impairment under iron deficiency was reported by Zimblet et al. for *tonB1* and *tonB2* deletion mutants of strain ATCC19606 (58). Since the authors of his study could not generate a *tonB3* deletion mutant by homologous recombination, the growth phenotype could not be assessed and the authors concluded on essentiality of the TonB3-ExbB3-ExbD3 system in *A. baumannii*. Whether this is due to experimental conditions or to differences in strain backgrounds is unclear. Supplementation with iron could restore the growth defects in their *tonB1* and *tonB2* mutants (58) as well as in our spontaneous *tonB3/exbD3* mutants of strain 307-0294 (Fig. 5). It remains to be determined if *tonB1* and *tonB2* mutants also show altered susceptibilities to siderophore-drug conjugates. All together the data suggest that *tonB* mutants, if selected *in vivo*, would be impaired in their fitness and probably be less virulent also in the patient, where iron availability is limited.

Both endogenous and heterologous overexpression of the *Ab-PiuA* and *Ab-PirA*, conferred increased susceptibility to both BAL30072 and MC-1 on *P. aeruginosa* strain PAO1 (Table 3). This establishes the ability of these two proteins to transport the two antibiotics; moreover it indicates the amount of *PiuA* and *PirA* expressed in PAO1 is probably the bottleneck for the transport of siderophore-drug conjugates rather than the availability of the TonB-ExbB/D systems. There must be a mutual recognition between the C-terminal part of the cytoplasmic membrane protein TonB in *P. aeruginosa* and the TonB-box located in the N-terminal domains of *PirA* and *PiuA* from *A. baumannii*. In *P. aeruginosa* the energy-coupling to iron-transporting TBDRs is mediated by TonB1 (67), while our data suggest that TonB3 is the equivalent protein in *A. baumannii*. However, TonB1 (*Pa*) and TonB3 (*Ab*) show only limited

amino acid sequence identity. The TonB3 domain of *A. baumannii* displayed the highest sequence similarity with the C-terminal regions of TolA (aa 277-322) (48% identity) and TonB2 (aa 178-223, 39% identity) of *P. aeruginosa*. These domains are located in the periplasm and thought to interact with the corresponding TBDR in the outer membrane (68). Which TonB protein of *P. aeruginosa* is indeed interacting with PiuA and PirA from *A. baumannii* remains to be determined. To our knowledge this is the first report on a heterologous complementation between TonB-dependent receptors in Gram-negative non-fermenters.

In summary, the previously uncharacterized TBDRs PiuA and PirA are the major uptake systems for the siderophore-drug conjugates BAL30072 and MC-1 in *A. baumannii*. Despite their overall similar crystal structure, differences in the external loops of the plug domain, could be important for substrate selectivity. We obtained evidence for heterologous recognition between a TonB protein(s) of *P. aeruginosa* and TBDRs of *A. baumannii*. Our study highlights the potential of siderophore-drug conjugates as an efficient strategy to increase antimicrobial transport into Gram-negative bacteria.

Acknowledgements.

We are grateful to R.A. Alm and S. Mills from Astra Zeneca (Waltham, MA, USA), who performed the whole genome sequencing of the *A. baumannii* mutants. Part of this work was presented at the ECCMID conference 2015, Copenhagen. The research leading to these results was conducted as part of the Translocation consortium (www.translocation.com) and has received support from the Innovative Medicines Joint Undertaking under *Grant Agreement* n°115525, resources which are composed of financial contribution from the European Union's seventh framework programme (FP7/2007-2013) and EFPIA companies in kind contribution.

489 **Supporting Information**

490 S1 Fig. Structural comparison between a) *Pa*-PiuA and Ab-PiuA, b) *Ab*-PiuA and *Ab*-PirA, c)
491 *Ab*-PirA and *Ec*-FepA, d) *Ab*-PiuA and *Ec*-FhuA

492 S2 Fig. Genetic organization of the three TonB systems in *A. baumannii*

493 S1 Table. Primers used in this study.

494 S2 Table. Crystallographic data and refinement statistics.

495

496

497 **Table 1. Bacterial strains and plasmids**

Strains/plasmid	Relevant characteristics	Reference, source
<i>P. aeruginosa</i>		
PAO1	PAO1, <i>mexT</i> non-functional	Laboratory collection
PAO1 Δ <i>piuA</i>	unmarked deletion of <i>piuA</i> gene	This study
<i>A. baumannii</i>		
ATCC19606	<i>A. baumannii</i> reference clinical isolate	HUG collection
307-0274	<i>A. baumannii</i> clinical isolate	T.A. Russo, SUNY, Buffalo
ATCC19606 Δ <i>piuA</i>	<i>piuA</i> (A1S_0474) deletion mutant	This study
ATCC19606 Δ <i>pirA</i>	<i>pirA</i> (A1S_0980) deletion mutant	This study
ATCC19606 Δ <i>piuA</i> Δ <i>pirA</i>	<i>piuA</i> , <i>pirA</i> double deletion mutant	This study
<i>E. coli</i>		
XL1-Blue	<i>recA1 endA1 gyrA96 thi-1 hsdR17</i> (r _K ⁻ m _K ⁺) <i>supE44 relA1 lac</i> [F' <i>proAB lac</i> ^R] Z Δ M15Tn10(Tc)]	Stratagene
ST18	<i>pro thi hsdR</i> ⁺ Tmp ^r Sm ^r ; chromosome::RP4-2 Tc::Mu-Kan::Tn7/ λ pir Δ <i>hemA</i>	(69)
Plasmids		
pMKm	contains a 1.7-kb Km cassette carrying <i>neo</i> gene, Km-R	(70)
pEX18Ap	gene replacement vector, Ap-R	(32)

pEX18Gm	gene replacement vector, Gm-R	(32)
pEX18Km	pEX18Ap derivate, 0.4-kb fragment of <i>bla</i> gene replaced with 1-kb <i>neo</i> gene from pMKm via AatII/Scal, Km-R	This study
pEX18Gm-pirA-ko	contains a 1.4-kb fusion fragment of the up- and downstream region of <i>pirA</i> , Gm-R	This study
pEX18Km-piuA-ko	1.1-kb fusion fragment of the 5' and 3' region of <i>piuA</i> , Km-R	This study
pEX1.8	Inducible expression vector, Ap-R	(71)
pIApX2	Broad-host range expression vector, Ap-R	I. Attree (Grenoble)
ppiuA1.1	<i>piuA</i> from PAO1 cloned into pIApX2, Ap-R	This study
ppirA1.1	<i>pirA</i> from PAO1 cloned into pIApX2, Ap-R	This study
ppiuA-Ab6.3	<i>piuA</i> -Ab cloned into pEX1.8, Ap-R	This study
ppirA-Ab4.1	<i>pirA</i> -Ab cloned into pIApX2, Ap-R	This study

^a Ap, ampicillin; Gm, gentamicin; Km, kanamycin; Sm, streptomycin, Tc, tetracycline; Tmp, trimethoprim.

HUG, Hôpitaux Universitaires de Genève

502 **TABLE 2.** Susceptibility of *piuA* and *pirA* deletion mutants of *A. baumannii*

Strain	MIC (mg/L)		
	BAL 30072	MC-1	ATM
ATCC19606	0.25	1	32
ATCC19606 $\Delta piuA$	1	2	32
ATCC19606 $\Delta pirA$	1-2	4	32
ATCC19606 $\Delta pirA \Delta piuA$	2-4	32	32

503 ATM, aztreonam

504

TABLE 3. Effects of heterologous expression of *Ab-PiuA* and *Ab-PirA* in *P. aeruginosa* PAO1 and PAO1 Δ *piuA* on susceptibility to monocyclic beta-lactam antibiotics

Strain	MIC (mg/L) ^a		
	BAL30072	MC-1	ATM
PAO1	1-2	0.5	4
+ pEX1.8	2	0.25	4
+ pIApX2	1	0.5	8
+ <i>ppiuA</i> 1.1 (<i>Pa</i>)	0.125	ND	4
+ <i>ppiuA</i> Δ L1.1 (<i>Pa</i>)	2	ND	4
+ <i>ppiuA</i> -Ab6.3	0.25	0.06	4
+ <i>ppirA</i> 1.1 (<i>Pa</i>)	0.25	ND	8
+ <i>ppirA</i> -Ab4.1	0.06	0.03	4
PAO1Δ<i>piuA</i>	8-16	2	4
+ pIApX2	16	4	8
+ pEX1.8	16	4	4
+ <i>ppiuA</i> 1.1 (<i>Pa</i>)	0.125	0.03	8
+ <i>ppiuA</i> -Ab6.3	8	2	2
+ <i>ppirA</i> 1.1 (<i>Pa</i>)	0.25	0.06	8
+ <i>ppirA</i> -Ab4.1	0.25	0.125	4

^a Determined in MH medium supplemented with carbenicillin at 100 mg/L and with 1 mM IPTG for strains harboring pEX1.8 and *ppiuA*-Ab6.3. ATM, aztreonam

511 **TABLE 4.** Susceptibility of *A. baumannii* mutants selected on BAL30072

Strain	MIC (mg/L)			Mutation ¹
	BAL30072	MC-1	ATM	
307-0294	0.25	1	32	wt
307-0294-R4	>8	>8	16	ExbD3 (Q4fs)
307-0294-R5	>8	>8	16	TonB3 (K106fs)
307-0294-R6	>8	>8	16	TonB3 (K80fs)

512 ¹fs, frame shift

513

514 **FIG 1** Chromosomal loci of *piuA* and *pirA* genes in *A. baumannii*, *P. aeruginosa* and *E. coli*.
515 The TBDR gene *piuA* is co-localized with the Fe(II)-dependent oxidoreductase gene *piuC*,
516 while the *pirA* locus differs among the three organisms. Only genes relevant for the study
517 context are shown.

518 **FIG 2 Structure-based sequence alignment of PiuA and PirA proteins from *P. aeruginosa***
519 **(*Pa*) and *A. baumannii* (*Ab*).** Secondary structure elements of *Ab*-PiuA are illustrated above
520 the alignment. Regions predicted to be involved in the binding of the siderophores are
521 highlighted by red boxes. Residues 'spatially' equivalent to those involved in substrate binding
522 in FhuA, FptA, FpvA are highlighted in green. Key residues of the secondary binding site of
523 FepA and conserved in the PirA structure are shown in yellow. Positions of residues of the
524 non-conserved initial binding site are highlighted by orange triangles. A cyan box highlights
525 the plug domain. The alignment was drawn using Aline (72).

526 **FIG 3 Crystal structures of PiuA and PirA from *P. aeruginosa* (*Pa*) and *A. baumannii***
527 **(*Ab*).** β -barrels are colored in green and N-terminal plug domains in blue. Loops NL1, NL2 and
528 NL3 of the plug domains are shown in red. Residues likely to be part of the siderophore
529 substrate binding site are shown as yellow sticks. Last solved residues of the flexible loops are
530 represented as spheres.

531 **FIG 4 Putative binding sites in PiuA of *P. aeruginosa* (*Pa*) and *A. baumannii* (*Ab*) and**
532 **PirA of *A. baumannii*.** The color scheme is as shown in Figure 3. The phosphate ion present
533 in the *Ab*-PiuA structure is colored in orange and red and residues Asp303 and Glu73 that
534 coordinate it are represented in green and white sticks.

535 **FIG 5 Growth of spontaneous mutants with decreased susceptibility to BAL30072.**
536 Strains were grown in MH-broth (MHB) with or without Fe(II)Cl₂ supplementation (20 μ M final
537 concentration). Growth was followed in a plate reader with regular OD₆₀₀ readings. The data
538 represent the average OD₆₀₀ value for duplicate cultures. Experiments were repeated on three

539 different occasions yielding similar results. Data from one representative experiment are
540 shown. Asterisks indicate frameshift mutations.

541

542

543

544 **References**

545

- 546 1. **Li XZ, Plesiat P, Nikaido H.** 2015. The challenge of efflux-mediated antibiotic resistance in
547 Gram-negative bacteria. *Clin Microbiol Rev* **28**:337-418.
- 548 2. **Ji C, Juarez-Hernandez RE, Miller MJ.** 2012. Exploiting bacterial iron acquisition: siderophore
549 conjugates. *Future Med Chem* **4**:297-313.
- 550 3. **Schalk IJ, Mislin GL, Brillet K.** 2012. Structure, function and binding selectivity and
551 stereoselectivity of siderophore-iron outer membrane transporters. *Curr Top Membr* **69**:37-
552 **66. doi: 10.1016/B978-0-12-394390-3.00002-1**:37-66.
- 553 4. **Schauer K, Rodionov DA, de Reuse H.** 2008. New substrates for TonB-dependent transport:
554 do we only see the 'tip of the iceberg'? *Trends Biochem Sci* **33**:330-338.
- 555 5. **Neidhardt FC, Bloch PL, Smith DF.** 1974. Culture medium for enterobacteria. *J Bacteriol*
556 **119**:736-747.
- 557 6. **Reynolds PR, Mottur GP, Bradbeer C.** 1980. Transport of vitamin B12 in *Escherichia coli*. Some
558 observations on the roles of the gene products of BtuC and TonB. *J Biol Chem* **255**:4313-4319.
- 559 7. **Wencewicz TA, Miller MJ.** 2013. Biscatecholate-monohydroxamate mixed ligand siderophore-
560 carbacephalosporin conjugates are selective sideromycin antibiotics that target *Acinetobacter*
561 *baumannii*. *J Med Chem* **56**:4044-4052.
- 562 8. **Ji C, Miller PA, Miller MJ.** 2012. Iron transport-mediated drug delivery: practical syntheses and
563 *in vitro* antibacterial studies of tris-catecholate siderophore-aminopenicillin conjugates reveals
564 selectively potent antipseudomonal activity. *J Am Chem Soc* **20**;134:9898-9901.
- 565 9. **Maejima T, Inoue M, Mitsuhashi S.** 1991. *In vitro* antibacterial activity of KP-736, a new
566 cephem antibiotic. *Antimicrob Agents Chemother* **35**:104-110.
- 567 10. **Kohira N, West J, Ito A, Ito-Horiyama T, Nakamura R, Sato T, Rittenhouse S, Tsuji M, Yamano**
568 **Y.** 2015. *In vitro* antimicrobial activity of siderophore cephalosporin S-649266 against

569 Enterobacteriaceae clinical isolates including carbapenem-resistant strains. Antimicrob Agents
570 Chemother **60**:729-734.

571 11. **Ito A, Kohira N, Bouchillon SK, West J, Rittenhouse S, Sader HS, Rhomberg PR, Jones RN,**
572 **Yoshizawa H, Nakamura R, Tsuji M, Yamano Y.** 2016. In vitro antimicrobial activity of S-
573 649266, a catechol-substituted siderophore cephalosporin, when tested against non-
574 fermenting Gram-negative bacteria. J Antimicrob Chemother **71**:670-677.

575 12. **Nikaido H, Rosenberg EY.** 1990. Cir and Fiu proteins in the outer membrane of *Escherichia coli*
576 catalyze transport of monomeric catechols: study with beta-lactam antibiotics containing
577 catechol and analogous groups. J Bacteriol **172**:1361-1367.

578 13. **Curtis NA, Eisenstadt RL, East SJ, Cornford RJ, Walker LA, White AJ.** 1988. Iron-regulated outer
579 membrane proteins of *Escherichia coli* K-12 and mechanism of action of catechol-substituted
580 cephalosporins. Antimicrob Agents Chemother **32**:1879-1886.

581 14. **Page MG, Dantier C, Desarbre E.** 2010. In vitro properties of BAL30072, a novel siderophore
582 sulfactam with activity against multiresistant gram-negative bacilli. Antimicrob Agents
583 Chemother **54**:2291-2302.

584 15. **McPherson CJ, Aschenbrenner LM, Lacey BM, Fahnoe KC, Lemmon MM, Finegan SM,**
585 **Tadakamalla B, O'Donnell JP, Mueller JP, Tomaras AP.** 2012. Clinically-Relevant Gram-
586 negative Resistance Mechanisms have no Effect on the Efficacy of MC-1, a Novel Siderophore-
587 Conjugated Monocarbam. Antimicrob Agents Chemother **56**:6334-6342.

588 16. **Han S, Caspers N, Zaniewski RP, Lacey BM, Tomaras AP, Feng X, Geoghegan KF,**
589 **Shanmugasundaram V.** 2011. Distinctive attributes of beta-lactam target proteins in
590 *Acinetobacter baumannii* relevant to development of new antibiotics. J Am Chem Soc
591 **133**:20536-20545.

592 17. **Mima T, Kvitko BH, Rholl DA, Page MG, Desarbre E, Schweizer HP.** 2011. In vitro activity of
593 BAL30072 against *Burkholderia pseudomallei*. Int J Antimicrob Agents **38**:157-159.

- 594 18. **Russo TA, Page MG, Beanan JM, Olson R, Hujer AM, Hujer KM, Jacobs M, Bajaksouzian S,**
595 **Endimiani A, Bonomo RA.** 2011. In vivo and in vitro activity of the siderophore monosulfactam
596 BAL30072 against *Acinetobacter baumannii*. *J Antimicrob Chemother* **66**:867-873.
- 597 19. **Dijkshoorn L, Nemec A, Seifert H.** 2007. An increasing threat in hospitals: multidrug-resistant
598 *Acinetobacter baumannii*. *Nat Rev Microbiol* **5**:939-951.
- 599 20. **Bou G, Martinez-Beltran J.** 2000. Cloning, nucleotide sequencing, and analysis of the gene
600 encoding an AmpC beta-lactamase in *Acinetobacter baumannii*. *Antimicrob Agents Chemother*
601 **44**:428-432.
- 602 21. **Bonnin RA, Nordmann P, Poirel L.** 2013. Screening and deciphering antibiotic resistance in
603 *Acinetobacter baumannii*: a state of the art. *Expert Rev Anti Infect Ther* **11**:571-583.
- 604 22. **Potron A, Poirel L, Nordmann P.** 2015. Emerging broad-spectrum resistance in *Pseudomonas*
605 *aeruginosa* and *Acinetobacter baumannii*: Mechanisms and epidemiology. *Int J Antimicrob*
606 *Agents* **45**:568-585.
- 607 23. **Magnet S, Courvalin P, Lambert T.** 2001. Resistance-nodulation-cell division-type efflux pump
608 involved in aminoglycoside resistance in *Acinetobacter baumannii* strain BM4454. *Antimicrob*
609 *Agents Chemother* **45**:3375-3380.
- 610 24. **Damier-Piolle L, Magnet S, Bremont S, Lambert T, Courvalin P.** 2008. AdeIJK, a resistance-
611 nodulation-cell division pump effluxing multiple antibiotics in *Acinetobacter baumannii*.
612 *Antimicrob Agents Chemother* **52**:557-562.
- 613 25. **Coyne S, Rosenfeld N, Lambert T, Courvalin P, Perichon B.** 2010. Overexpression of resistance-
614 nodulation-cell division pump AdeFGH confers multidrug resistance in *Acinetobacter*
615 *baumannii*. *Antimicrob Agents Chemother* **54**:4389-4393.
- 616 26. **Koebnik R.** 2005. TonB-dependent trans-envelope signalling: the exception or the rule? *Trends*
617 *Microbiol* **13**:343-347.
- 618 27. **Funahashi T, Tanabe T, Mihara K, Miyamoto K, Tsujibo H, Yamamoto S.** 2012. Identification
619 and characterization of an outer membrane receptor gene in *Acinetobacter baumannii*

required for utilization of desferricoprogen, rhodotorulic acid, and desferrioxamine B as xenosiderophores. Biol Pharm Bull **35**:753-760.

28. **Mihara K, Tanabe T, Yamakawa Y, Funahashi T, Nakao H, Narimatsu S, Yamamoto S.** 2004. Identification and transcriptional organization of a gene cluster involved in biosynthesis and transport of acinetobactin, a siderophore produced by *Acinetobacter baumannii* ATCC 19606T. Microbiology **150**:2587-2597.
29. **Yamamoto S, Okujo N, Sakakibara Y.** 1994. Isolation and structure elucidation of acinetobactin, a novel siderophore from *Acinetobacter baumannii*. Arch Microbiol **162**:249-254.
30. **Zimblar DL, Penwell WF, Gaddy JA, Menke SM, Tomaras AP, Connerly PL, Actis LA.** 2009. Iron acquisition functions expressed by the human pathogen *Acinetobacter baumannii*. Biometals **22**:23-32.
31. **Anonymous.** 2009. Clinical and Laboratory Standards Institute.. Methods for dilution antimicrobial susceptibility tests for bacteria that grow aerobically., vol Eighth Edition. Approved standard M7-A8.CLSI, Wayne, PA, USA.
32. **Hoang TT, Karkhoff-Schweizer RR, Kutchma AJ, Schweizer HP.** 1998. A broad-host-range Flp-FRT recombination system for site-specific excision of chromosomally-located DNA sequences: application for isolation of unmarked *Pseudomonas aeruginosa* mutants. Gene **212**:77-86.
33. **Pletzer D, Lafon C, Braun Y, Köhler T, Page MG, Mourez M, Weingart H.** 2014. High-throughput screening of dipeptide utilization mediated by the ABC transporter DppBCDF and its substrate-binding proteins DppA1-A5 in *Pseudomonas aeruginosa*. PLoS ONE **9**:e111311.
34. **Liu H, Naismith JH.** 2008. An efficient one-step site-directed deletion, insertion, single and multiple-site plasmid mutagenesis protocol. BMC Biotechnol **8**:91.
35. **Bryksin AV, Matsumura I.** 2010. Rational design of a plasmid origin that replicates efficiently in both gram-positive and gram-negative bacteria. PLoS ONE **5**:e13244.

- 645 36. **Petersen TN, Brunak S, von Heijne G, Nielsen H.** 2011. SignalP 4.0: discriminating signal
646 peptides from transmembrane regions. *Nat Methods* **8**:785-786.
- 647 37. **Liu J, Wolfe AJ, Eren E, Vijayaraghavan J, Indic M, van den BB, Movileanu L.** 2012. Cation
648 selectivity is a conserved feature in the OccD subfamily of *Pseudomonas aeruginosa*. *Biochim*
649 *Biophys Acta* **1818**:2908-2916.
- 650 38. **Winter G.** 2010. xia2: an expert system for macromolecular crystallography data reduction. *J*
651 *Appl Crystallogr* **43**:186-190.
- 652 39. **Zhang Z, Sauter NK, van den Bedem H, Snell G, Deacon AM.** 2006. Automated diffraction
653 image analysis and spot searching for high-throughput crystal screening. *J Appl Crystallogr*
654 **39**:112-119.
- 655 40. **Sauter NK, Grosse-Kunstleve RW, Adams PD.** 2004. Robust indexing for automatic data
656 collection. *J Appl Crystallogr* **37**:399-409.
- 657 41. **Kabsch W.** 1993. Automatic processing of rotation diffraction data from crystals of initially
658 unknown symmetry and cell constants. *J Appl Crystallogr* **26**:795-800.
- 659 42. **Evans P.** 2006. Scaling and assessment of data quality. *Acta Crystallogr D Biol Crystallogr* **62**:72-
660 82.
- 661 43. **Ferguson AD, Hofmann E, Coulton JW, Diederichs K, Welte W.** 1998. Siderophore-mediated
662 iron transport: crystal structure of FhuA with bound lipopolysaccharide. *Science* **282**:2215-
663 2220.
- 664 44. **McCoy AJ, Grosse-Kunstleve RW, Adams PD, Winn MD, Storoni LC, Read RJ.** 2007. Phaser
665 crystallographic software. *J Appl Crystallogr* **40**:658-674.
- 666 45. **Buchanan SK, Smith BS, Venkatramani L, Xia D, Esser L, Palnitkar M, Chakraborty R, van der**
667 **HD, Deisenhofer J.** 1999. Crystal structure of the outer membrane active transporter FepA
668 from *Escherichia coli*. *Nat Struct Biol* **6**:56-63.
- 669 46. **Emsley P, Cowtan K.** 2004. Coot: model-building tools for molecular graphics. *Acta Crystallogr*
670 *D Biol Crystallogr* **60**:2126-2132.

- 671 47. **Murshudov GN, Vagin AA, Dodson EJ.** 1997. Refinement of macromolecular structures by the
672 maximum-likelihood method. *Acta Crystallogr D Biol Crystallogr* **53**:240-255.
- 673 48. **Chen VB, Arendall WB, III, Headd JJ, Keedy DA, Immormino RM, Kapral GJ, Murray LW,**
674 **Richardson JS, Richardson DC.** 2010. MolProbity: all-atom structure validation for
675 macromolecular crystallography. *Acta Crystallogr D Biol Crystallogr* **66**:12-21.
- 676 49. **Van Delden C, Page MG, Kohler T.** 2013. Involvement of Fe uptake systems and AmpC beta-
677 lactamase in susceptibility to the siderophore monosulfactam BAL30072 in *Pseudomonas*
678 *aeruginosa*. *Antimicrob Agents Chemother* **57**:2095-2102.
- 679 50. **Higgins PG, Stefanik D, Page MG, Hackel M, Seifert H.** 2012. In vitro activity of the siderophore
680 monosulfactam BAL30072 against meropenem-non-susceptible *Acinetobacter baumannii*. *J*
681 *Antimicrob Chemother* **67**:1167-1169.
- 682 51. **Eijkelkamp BA, Hassan KA, Paulsen IT, Brown MH.** 2011. Investigation of the human pathogen
683 *Acinetobacter baumannii* under iron limiting conditions. *BMC Genomics* **12**:126. doi:
684 **10.1186/1471-2164-12-126.**:126-12.
- 685 52. **Aravind L, Koonin EV.** 2001. The DNA-repair protein AlkB, EGL-9, and leprecan define new
686 families of 2-oxoglutarate- and iron-dependent dioxygenases. *Genome Biol* **2**:RESEARCH0007.
- 687 53. **Zimble DL, Park TM, Arivett BA, Penwell WF, Greer SM, Woodruff TM, Tierney DL, Actis LA.**
688 2012. Stress response and virulence functions of the *Acinetobacter baumannii* NfuA Fe-S
689 scaffold protein. *J Bacteriol* **194**:2884-2893.
- 690 54. **Ghysels B, Ochsner U, Mollman U, Heinisch L, Vasil M, Cornelis P, Matthijs S.** 2005. The
691 *Pseudomonas aeruginosa pirA* gene encodes a second receptor for ferrienterobactin and
692 synthetic catecholate analogues. *FEMS Microbiol Lett* **246**:167-174.
- 693 55. **Cobessi D, Celia H, Pattus F.** 2005. Crystal structure at high resolution of ferric-pyochelin and
694 its membrane receptor FptA from *Pseudomonas aeruginosa*. *J Mol Biol* **352**:893-904.

- 695 56. **Cobessi D, Celia H, Folschweiller N, Schalk IJ, Abdallah MA, Pattus F.** 2005. The crystal
696 structure of the pyoverdine outer membrane receptor FpvA from *Pseudomonas aeruginosa* at
697 3.6 angstroms resolution. *J Mol Biol* **347**:121-134.
- 698 57. **Krissinel E, Henrick K.** 2004. Secondary-structure matching (SSM), a new tool for fast protein
699 structure alignment in three dimensions. *Acta Crystallogr D Biol Crystallogr* **60**:2256-2268.
- 700 58. **Zimblar DL, Arivett BA, Beckett AC, Menke SM, Actis LA.** 2013. Functional features of TonB
701 energy transduction systems of *Acinetobacter baumannii*. *Infect Immun* **81**:3382-3394.
- 702 59. **Van Delden C, Page MG, Köhler T.** 2013. Involvement of Fe uptake systems and AmpC beta-
703 lactamase in susceptibility to the siderophore monosulfactam BAL30072 in *Pseudomonas*
704 *aeruginosa*. *Antimicrob Agents Chemother* **57**:2095-2102.
- 705 60. **Zheng T, Nolan EM.** 2014. Enterobactin-mediated delivery of beta-lactam antibiotics enhances
706 antibacterial activity against pathogenic *Escherichia coli*. *J Am Chem Soc* **136**:9677-9691.
- 707 61. **Zheng T, Bullock JL, Nolan EM.** 2012. Siderophore-mediated cargo delivery to the cytoplasm
708 of *Escherichia coli* and *Pseudomonas aeruginosa*: syntheses of monofunctionalized
709 enterobactin scaffolds and evaluation of enterobactin-cargo conjugate uptake. *J Am Chem Soc*
710 **134**:18388-18400.
- 711 62. **Chimento DP, Kadner RJ, Wiener MC.** 2005. Comparative structural analysis of TonB-
712 dependent outer membrane transporters: implications for the transport cycle. *Proteins*
713 **59**:240-251.
- 714 63. **Payne MA, Igo JD, Cao Z, Foster SB, Newton SM, Klebba PE.** 1997. Biphasic binding kinetics
715 between FepA and its ligands. *J Biol Chem* **272**:21950-21955.
- 716 64. **Cao Z, Qi Z, Sprencel C, Newton SM, Klebba PE.** 2000. Aromatic components of two ferric
717 enterobactin binding sites in *Escherichia coli* FepA. *Mol Microbiol* **37**:1306-1317.
- 718 65. **Annamalai R, Jin B, Cao Z, Newton SM, Klebba PE.** 2004. Recognition of ferric catecholates by
719 FepA. *J Bacteriol* **186**:3578-3589.

720 66. **Newton SM, Igo JD, Scott DC, Klebba PE.** 1999. Effect of loop deletions on the binding and
721 transport of ferric enterobactin by FepA. *Mol Microbiol* **32**:1153-1165.

722 67. **Shirley M, Lamont IL.** 2009. Role of TonB1 in pyoverdine-mediated signaling in *Pseudomonas*
723 *aeruginosa*. *J Bacteriol* **191**:5634-5640.

724 68. **Chu BC, Peacock RS, Vogel HJ.** 2007. Bioinformatic analysis of the TonB protein family.
725 *Biometals* **20**:467-483.

726 69. **Thoma S, Schobert M.** 2009. An improved *Escherichia coli* donor strain for diparental mating.
727 *FEMS Microbiol Lett* **294**:127-132.

728 70. **Murillo J, Shen H, Gerhold D, Sharma A, Cooksey DA, Keen NT.** 1994. Characterization of
729 pPT23B, the plasmid involved in syringolide production by *Pseudomonas syringae* pv. *tomato*
730 PT23. *Plasmid* **31**:275-287.

731 71. **Pearson JP, Pesci EC, Iglewski BH.** 1997. Roles of *Pseudomonas aeruginosa las* and *rhl* quorum-
732 sensing systems in control of elastase and rhamnolipid biosynthesis genes. *J Bacteriol*
733 **179**:5756-5767.

734 72. **Bond CS, Schüttelkopf AW.** 2016. ALINE: a WYSIWYG protein-sequence alignment editor for
735 publication quality alignments. *Acta Crystallographica* **D65**:510-512.

736

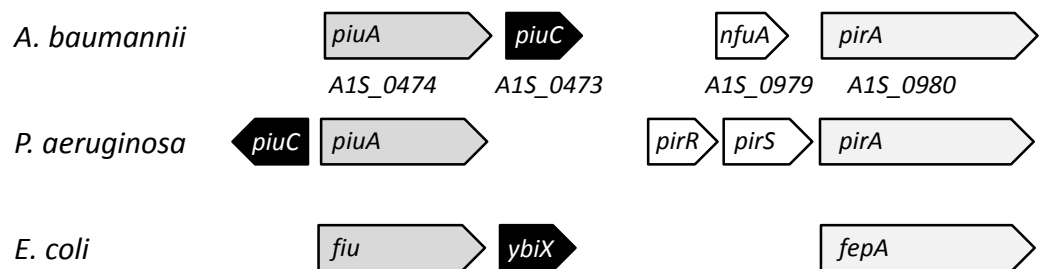


Fig. 1. Chromosomal loci of *piuA* and *pirA* genes in *A. baumannii*, *P. aeruginosa* and *E. coli*. The TBDR gene *piuA* is co-localized with the Fe(II)-dependent oxidoreductase gene *piuC*, while the *pirA* locus differs among the three organisms.

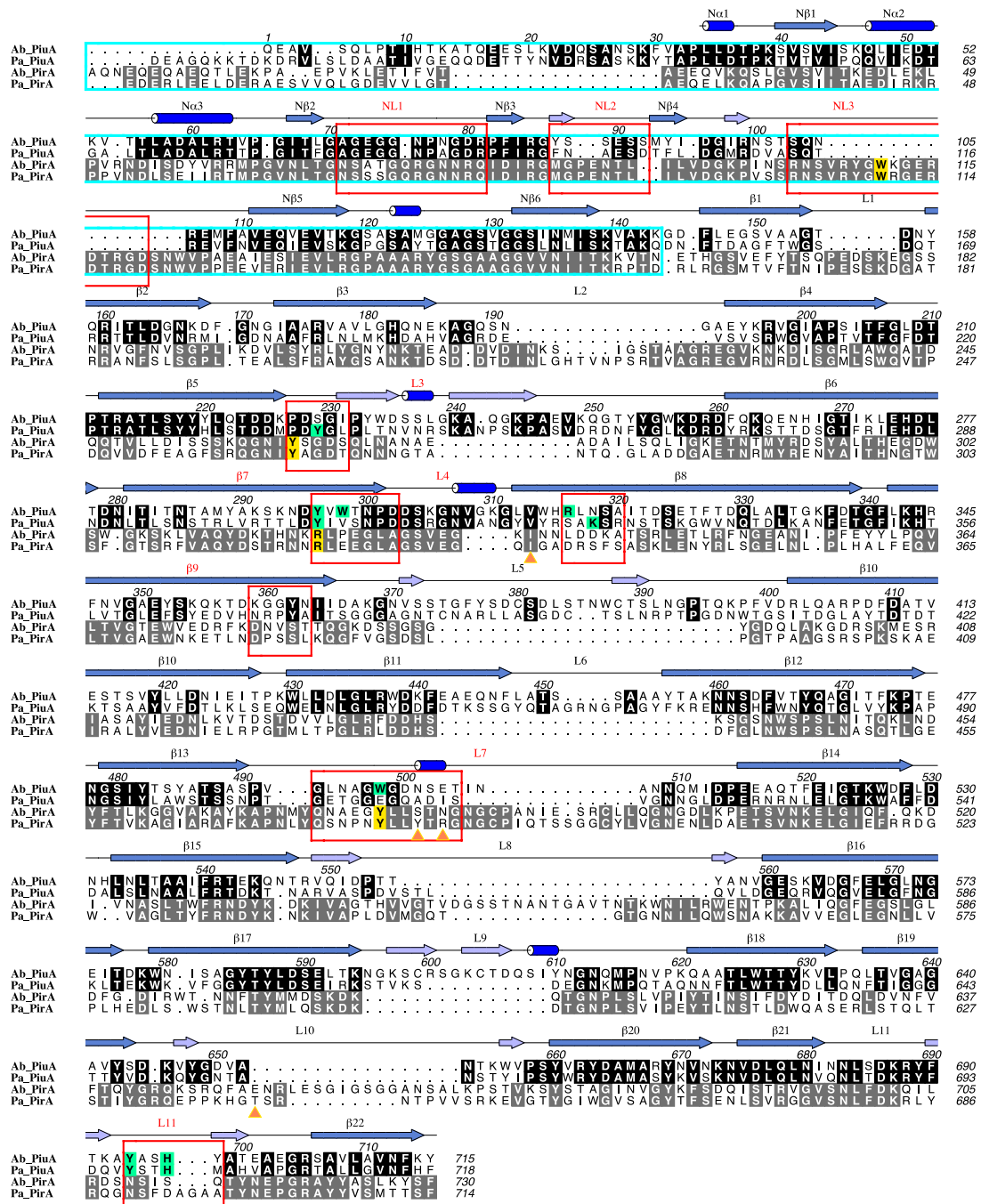


Fig. 2. Structure-based sequence alignment of PiuA and PirA proteins from *P. aeruginosa* (Pa) and *A. baumannii* (Ab). Secondary structure elements of Ab-PiuA are illustrated above the alignment. Regions predicted to be involved in the binding of the siderophores are highlighted by red boxes. Residues ‘spatially’ equivalent to those involved in substrate binding in FhuA, FptA, FpvA are highlighted in green. Key residues of the secondary binding site of FepA and conserved in the PirA structure are shown in yellow. A cyan box highlights the plug domain. The alignment was drawn using Aline.

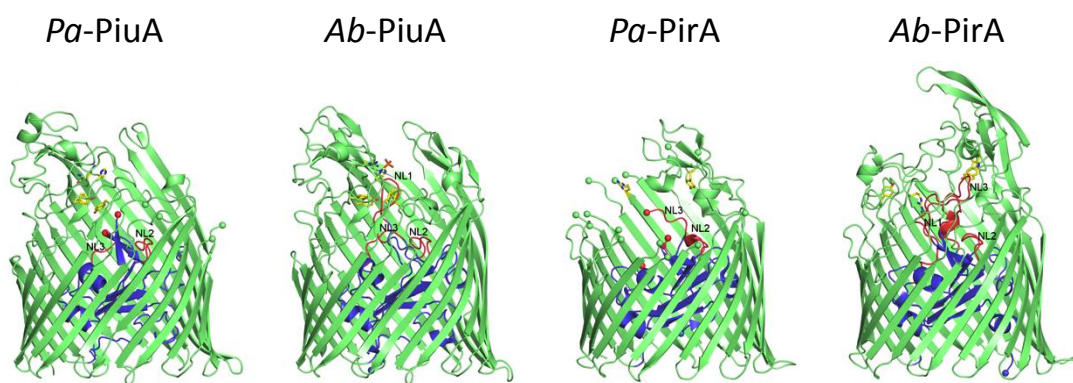


Fig. 3. Crystal structures of PiuA and PirA from *P. aeruginosa* (*Pa*) and *A. baumannii* (*Ab*). β -barrels are colored in green and N-terminal plug domains in blue. Loops NL1, NL2 and NL3 of the plug domains are shown in red. Residues likely to be part of the siderophore substrate binding site are shown as yellow sticks. Last solved residues of the flexible loops are represented as spheres.

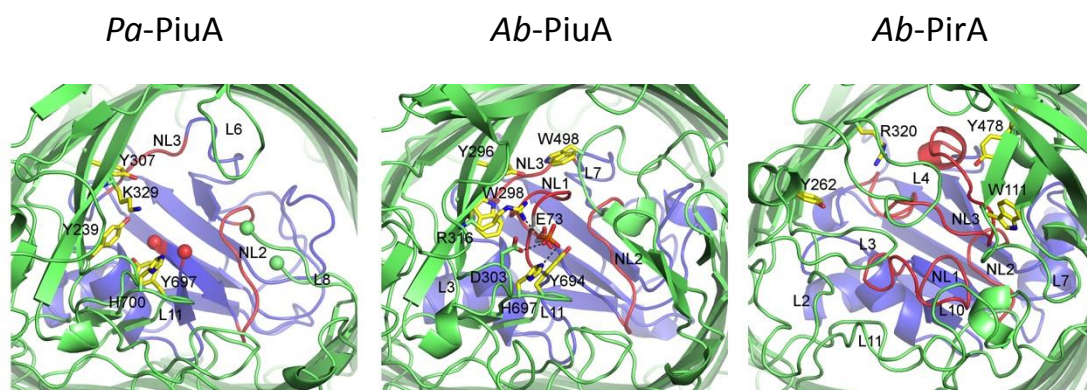


Fig. 4. Putative binding sites in PiuA of *P. aeruginosa* (*Pa*) and *A. baumannii* (*Ab*) and PirA of *A. baumannii*. The color scheme is as shown in Figure 3. The phosphate ion present in the *Ab*-PiuA structure is colored in orange and red and residues Asp303 and Glu73 that coordinate it are represented in green and white sticks.

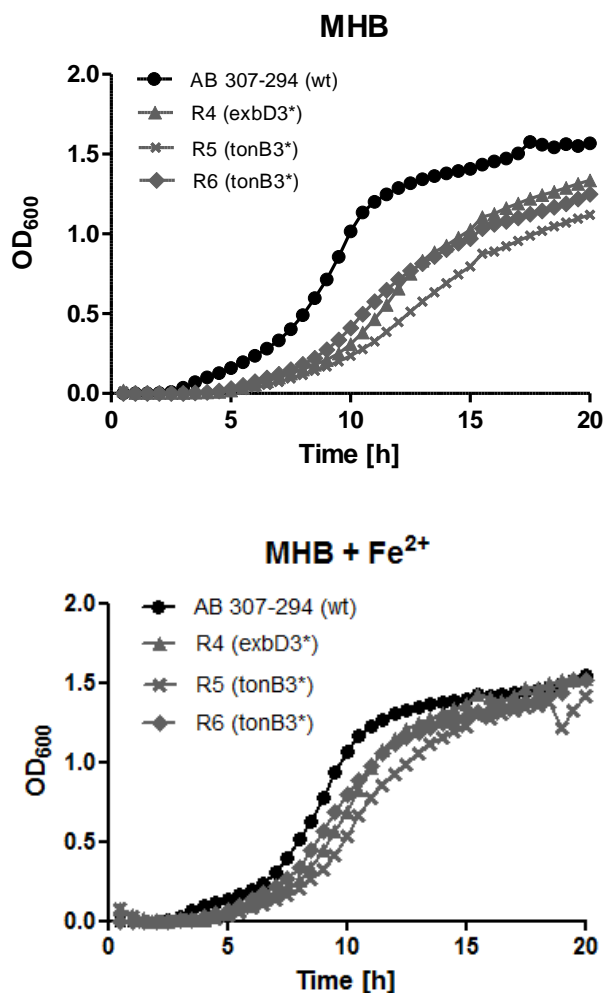


Fig. 5. Growth of spontaneous mutants with decreased susceptibility to BAL30072. Strains were grown in MH-broth (MHB) with or without Fe(II)Cl₂ supplementation (20 μM final concentration). Growth was followed in a plate reader with hourly OD₆₀₀ readings. The data represent the average OD₆₀₀ value for duplicate cultures. Experiments were repeated on three different occasions yielding similar results.